Journal of The Electrochemical Society, **164** (13) A2967-A2976 (2017)
0013-4651/2017/164(13)/A2967/10/$37.00 © The Electrochemical Society

Effect of Nano-Fillers on Capacity Retention and Rate Capability of Mesocarbon Microbeads Anode

Salahuddin Ahamad,[a,*] Mujeeb Ahmad,[b] Bodh Raj Mehta,[b] and Amit Gupta[a,,z]**

[a]*Department of Mechanical Engineering, Indian Institute of Technology Delhi, Hauz Khas, New Delhi 110016, India*
[b]*Department of Physics, Indian Institute of Technology Delhi, Hauz Khas, New Delhi 110016, India*

Thin film mesocarbon microbeads (MCMB) composite electrodes consisting of hybrid nano-fillers of carbon black (CB) and carbon nanotubes (CNT) have been developed and characterized by evaluating their electrical and electrochemical properties. The composite electrodes have been fabricated with various weight fractions of CB and CNT. It is shown that by partial replacement of CB by CNT in electrodes, a synergistic improvement in electrical conductivity, initial capacity and stability in cycling behavior at low (0.25C) as well as at high rates (4C) is achievable. This is attributed to the combined effect of (i) hybrid of CB-CNT providing short- and long-range conducting pathways by effectively filling the gaps between MCMB-MCMB, CNT-CNT and MCMB-CNT clusters, and (ii) formation of a compact and stable solid-electrolyte film resulting in a compact three-dimensional conducting scaffold. The electrodes with CB-CNT hybrid additives exhibit best performance in terms of capacity retention (342.8 $mAhg^{-1}$ after 50 cycles with almost 98% capacity retention at 0.25C and 280.0 $mAhg^{-1}$ after 100 cycles at 4C) and rate capability. This kind of approach to create a hybrid of geometrically distinct shape, aspect ratio and dispersion characteristics conducting fillers manifests a promising strategy to develop improved performance composite anodes for future lithium-ion batteries.
© 2017 The Electrochemical Society. [DOI: 10.1149/2.0351713jes] All rights reserved.

Manuscript submitted July 21, 2017; revised manuscript received September 14, 2017. Published September 28, 2017. This was Paper 583 presented at the New Orleans, Louisiana, Meeting of the Society, May 28–June 1, 2017.

The global lithium-ion battery industry is growing at an impressive rate and is expected to grow even further in the near future. The main reasons for this are the high energy density and excellent cycling performance that these batteries exhibit and that no other energy storage devices can match. Scientists and engineers all over the globe are experimenting with a handful of ideas that could make batteries vastly better than they are today, which could lead to more affordable electric cars and cheaper ways to store intermittent renewable energy.[1–4] Furthermore, fluctuating price of crude oil and a limited resource have forced more intense research directed toward partially or fully gasoline free vehicles. The use of lithium-ion batteries in the automotive sector has been receiving quite significant attention. Lithium-ion batteries have been very successful in the electronic market and have been used as viable and efficient power sources for many small and portable devices such as mobiles, laptop, watches, camcorders, PDAs, cameras and other communication devices. However, limitations of slow electronic conduction in electrodes have prohibited large scale commercialization of this energy storage technology in automotives (such as EVs, HEVs, PHEVs, etc.) where high power density is required.[5,6] In addition, improper contact due to large size of active materials makes it difficult to achieve their full theoretical capacities at practical level.

A number of methods have been adopted to improve the conductivity of active materials. Some of these are surface coating with conductive material, lattice doping and addition of metallic particles such as copper and nickel.[7–16] Traditionally, amorphous carbon black (CB) is used as conductive additive to fill the interspace between the electrode active particles.[17–20] However, the inability to form longer electronic pathways due to poor point-to-point connection of carbon black in the electrode matrix provides avenues for further improvement. Carbon nanotubes (CNT) have emerged as conductive additives for the lithium-ion battery electrodes because of their exceptional electronic and mechanical properties in comparison to carbon black.[20–23] Yang et al. reported that multiwalled carbon nanotubes (MWCNT) have conductivity 1–4 $\times$ 10^2 S/cm along the tube axis and 5–25 S/cm perpendicular to the tube axis,[24] whereas the conductivity of carbon black is 14 S/cm.[25] Moreover, due to their elongated structure, CNT could establish an efficient electrical network between the active particles that can hinder the agglomeration of active material in comparison to traditionally used carbonaceous additives and thus improve the electrochemical performance of composite electrodes.[26,27] However, experimentally reported electronic conductivity of composite electrodes with CNT is relatively low compared with the electronic conductivity expected by the simple rule of mixture.[28] This low value of electronic conductivity is caused by high contact resistance between CNT-CNT and high interfacial resistance between CNT and surrounding materials.[29] Such kind of contact resistance arises due to tunnelling effect and hence it also termed as tunnelling resistance. Although, it is easier for carbon black spherules to form a conductive layer on individual particle of active material by making point-to-point contact locally, these are unable to provide a long range conducting network. Thus, a conducting medium consisting of conducting additives with a wide range of aspect ratios appears to be a promising strategy to improve the electrical and electrochemical performance of electrodes in lithium-ion battery. It has been further reported that $LiCoO_2$ with Super P-SACNT conductive network stabilizes the cycling performance, alleviates polarization and helps avoid agglomeration of CNT.[5] A further investigation was carried out on carbon fibers and carbon black as hybrid conducting additives in $LiFePO_4$ cathode that exhibited better power performance with the mixture in comparison to electrodes containing only single conducting agent.[30] This strategy, i.e., tailoring the conducting network by using geometrically different conducting fillers was also applied to polymer nanocomposite system to enhance the thermal conductivity, electrical conductivity and piezoresistive sensitivity.[31–34]

A number of carbonaceous materials such as graphene, carbon nanotubes (CNTs), carbon nanofibers (CNFs), carbon nanobeads, hollow carbon nanospheres and porous carbon with surface functionalization (such as B, N and P) have been investigated as anodes for lithium-ion batteries with varying success.[35–42] However, the relatively large voltage slope and high lithium-inventory loss of these materials are some issues that remain to be addressed. The graphitic carbon is the most common anode material for lithium-ion battery anode.[43–45] Among them, the mesocarbon microbeads (MCMB) graphite material is one of the most promising anode material owing to its higher packing density, narrow particle size distribution (8–15 μm), and higher edge-plane surface than graphitic flakes. The diffusion kinetics of lithium-ion intercalation along the graphene layers is 4–6 order of magnitude higher than c-axis.[46] Thus, minimizing the basal plane surface and maximize the edge plane, i.e., engineering the crystallographic structure of graphitic material results in improving the kinetics of Li diffusion. Therefore, spherical shape particles of MCMB exhibit higher capacity retention and rate capabilities due to its higher edge-plane surface than graphite flakes.[38,47–49]

The stability of passivating layer (i.e., solid-electrolyte interface, SEI) formed on the surface of carbon electrode by the decomposition

*Electrochemical Society Student Member.
**Electrochemical Society Member.
[z]E-mail: agupta@mech.iitd.ac.in

Downloaded on 2017-09-28 to IP 103.27.9.249 address. Redistribution subject to ECS terms of use (see ecsdl.org/site/terms_use) unless CC License in place (see abstract).

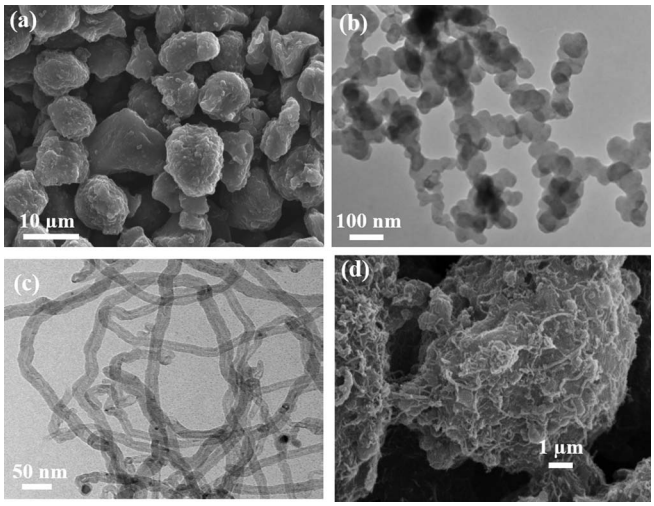

Figure 1. (a) SEM image of MCMB active material, (b) TEM image of Carbon Black (Super-P), (c) TEM image of MWCNT, and (d) SEM image of composite electrode with MWCNT and CB as additive.

of liquid electrolyte is the most crucial parameter in deciding the cycling performance of this anode. In the case of cathode, the kinetics of decomposition of electrolyte at the surface of cathode active material is different because of a higher operating potential for intercalation. Hence, increase of internal resistance, loss of electrical contact in the electrode, volume expansion of active material and surface layer formation in anode are factors that are quite different from that exhibited in cathodes. Due to these reasons, the role of additives in formation of the surface layer cannot be simply predicted by extrapolating inferences from examination of cathode electrochemical behavior to the carbon anode.

In this work, we investigate and emphasize the role of CNT and CB as individual or as a hybrid CB-CNT conductive filler on improving the electronic conductivity and electrochemical performance of MCMB electrodes. The most suitable composition of these fillers is quantified and the rate capability of the composite electrode when cycled under galvanostatic conditions used to evaluate capacity retention in MCMB anode. It is the first time that the effect of mixture of different aspect ratio conducting additives in MCMB anode for synergistic improvement in electronic conductivity, cycling stability and rate capability of this anode has been examined. We show that the use of CB-CNT hybrid filler leads to the formation of a three-dimensional hybrid network that offers faster electron conduction, helps in maintaining fairly uniform conduction of electrons over the discharge and charge cycle, a longer cycling stability and excellent rate capability of the MCMB anode. We propose that this happens due to a versatile charge transport in short- as well as long-range which is not possible with the use of only one type of nano-filler.

Experimental

Preparation and characterization of electrode.—MCMB, carbon black (Super-P, D_{mean}: 35 nm), carbon nanotubes, polyvinylidene fluoride (PVdF), polypropylene membrane (separator) and *N*-methyl-2-pyrrolidone (NMP) were procurred from Xiamen TOB New Energy Technology Co. Ltd., China. All the materials were used as purchased. Because of radial and near circumferential orientation of graphitic planes, MCMB allows fast diffusion of Li toward the center of the particle. The spherical shape particles of MCMB used in this work have average size of ca. 8 µm as shown in Fig. 1a. CB has been used extensively as a conductive additive in lithium-ion batteries having spherical morphology of primary particles which arrange themselves as fused particulate to form an aggregate of diameter 20–30 nm as shown in Fig. 1b. The carbon nanotubes used in this work were multi-walled (MWCNT) with an average diameter of about 10–30 nm (see Fig. 1c). The total content of conductive additives in each electrode was kept 4 wt% of total mass (*x* wt% of CB + *4-x* wt% of CNT where, $x = 0,1,2,3,4$). The electrode not containing CNT were treated as baseline. The composite electrodes were fabricated with the following composition: 88 wt% MCMB, 4 wt% conductive additive (CB and/or CNT) and 8 wt% PVdF, all on dry weight basis. A schematic illustration of the steps adopted to fabricate the working electrodes are shown in Fig. 2. First, the PVdF binder was dissolved in NMP solvent and mixed for 30 minutes in a vacuum mixer (MTI-Corp., CA, USA). Afterwards, the active material (MCMB) and CB were dry mixed using mortar and gradually added to the PVdF solution, with further mixing for 1 hour. In case of CNT, the MWCNT was mixed in NMP solvent and the suspension was sonicated using probe sonicator (Omni-inc., GA, USA) at a power level of 350 W to ensure complete disentanglement of CNT. The sonicated CNT-NMP solvent dispersion was mixed with a MCMB and additives in NMP. This mixture was further stirred under vacuum for 75 minutes for creating a homogenous dispersion before coating the slurry on copper substrate. As shown in Fig. 3, changing the sonication duration from 10 minutes

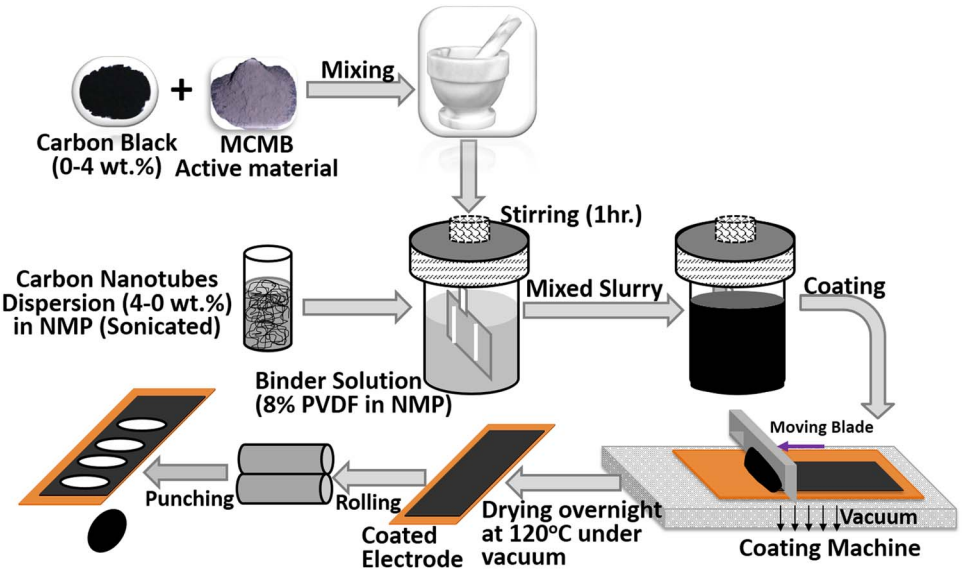

Figure 2. Schematic view for various steps followed for the electrode preparation.

Downloaded on 2017-09-28 to IP 103.27.9.249 address. Redistribution subject to ECS terms of use (see ecsdl.org/site/terms_use) unless CC License in place (see abstract).

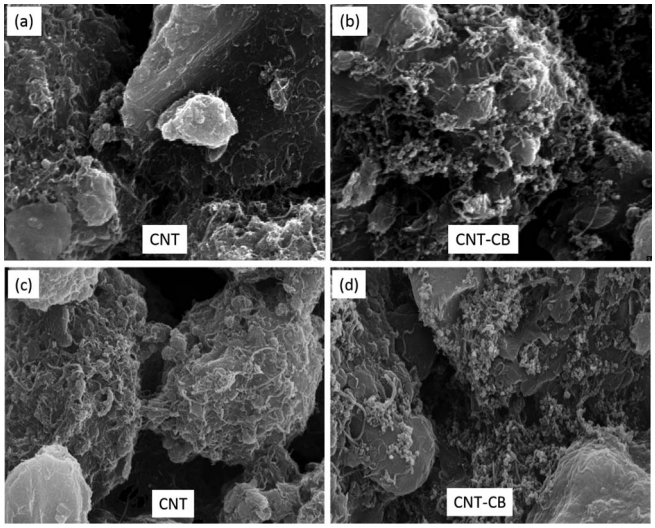

Figure 3. SEM images of MCMB composite electrode to illustrate the dispersion of nano-fillers CNT and CNT-CB for different sonication time (a) & (b) for 30 min. sonication (c) & (d) for 10 min sonication.

to 30 minutes had no significant difference on the distribution of CNT-CB in the composite electrode matrix. Once the slurry was prepared, it was coated on battery grade copper foil (thickness 15 μm) using height adjustable "doctor-blade" technique (MTI-Corp., CA, USA). After drying overnight at 120°C, the electrode laminates were calendered to about 15% of initial film thickness to ensure good contact between the electrode components as well as between the electrode mass and the current collector using roll press (MTI-Corp., CA, USA). Then, electrode discs with diameter of 12 mm were punched from the calendered laminate. The disks were dried in vacuum oven at 80°C for 4 hours before transferring it to a glove box for cell assembly.

The morphologies and microstructure of active material, conductive additives and composite electrode were analyzed using S–4800 field emission scanning electron microscope (FESEM) (Hitachi Co. Ltd., Japan) operated at 3.0 kV and high-resolution transmission electron microscope (HRTEM; Tecnai TF20, FEI, USA) operated at 200 kV. The corresponding X-ray diffraction (XRD) analysis was conducted on a Rigaku D/max-2500VB system (Rigaku Co., Tokyo, Japan) using Cu/K_α radiation ($\lambda = 1.5406$ Å). Finally, the MWCNT and CB were characterized by Raman spectroscopy (Renishaw Raman System, Invia, UK) with a laser excitation energy corresponding to 514 nm.

The in-plane electrical conductivity measurement was performed by using Seebeck & electric resistivity unit (model LSR-3, Linseis) at 25°C. In order to measure the electrical conductivity of electrode nanocomposite, the films were compressed to 15% of its initial thickness to ensure proper contact between different phases. Afterwards, the calandered films were cut into small rectangular sizes (15 mm × 5 mm × 0.3 mm) and finally the specimens were transferred to silica substrate by using an epoxy adhesive.

Cell assembly and electrochemical testing.—The two-electrode CR2016 coin type half-cells were assembled in a vacuum glove box (Jacomex SAS, France) with both moisture and oxygen level below 0.5 ppm. A porous polypropylene film (thickness: 25 μm) and 1M $LiPF_6$ solution in a mixture of ethylene carbonate (EC) and dimethyl carbonate (DMC) mixed at volume ratio of 1:1 (Sigma-Aldrich) were used as the separator and electrolyte, respectively. A Li-metal foil with 16 mm diameter and 400 μm thickness was used as counter and reference electrode. Finally, the cells were sealed by electric coin cell crimping machine (MTI-Corp., CA, USA). After assembly, the cells were kept at rest for 4 hours to ensure complete percolation of electrolyte through the pores.

The galvanostatic charge-discharge cycling of cells was performed using a Biologic VMP-3 testing workstation with cutoff potential of 0.005–2.0 V vs. Li/Li^+ at 0.25C, 1C and 4C (equals to 93, 372 and 1488 mAg^{-1} respectively; calculated using the theoretical capacity of graphite as 372 $mAhg^{-1}$). The cyclic voltammogram were obtained over a voltage range of 0.0–2.0 V at the scan rate of 0.1 mV s^{-1} using Biologic VMP-3. The electrochemical impedance spectroscopy (EIS) measurement was performed in the frequency range 5 mHz–200 kHz, and the applied bias voltage was set at open circuit voltage with 5 mV AC amplitude between the counter and working electrodes using Biologic VMP-3. All electrochemical experiments were carried out at a working temperature of 25°C.

Results and Discussion

Physical characterization.—The morphology and structure of MCMB active material, conductive additives (CB and CNT) and composite electrode were characterized by SEM and TEM and their images are shown in Fig. 1. It can be observed from Fig. 1a that particle size of MCMB spherules is in the range 8–15 μm. Carbon black (CB) particles are aggregates that consisted of spherical primary nanoparticles in the range of 20–30 nm (Fig. 1b). As shown in Fig. 1c the average outer diameter and the aspect ratio of CNT used in this study are ca.10–30 nm and ca. 100–500, respectively and they form an entangled structure. The SEM image of nanocomposite electrode with MCMB-CB-CNT scaffold is shown in Fig. 1d. Most CNT connect multiple MCMB particles and extend throughout the composite electrode, whereas CB spherules, due to their nano-size and spherical morphology, are distributed mainly in the gaps among MCMB particles between MCMB-CNT and CNT-CNT.

The structural differences of conductive additives, CNT and CB, were investigated by XRD and Raman spectroscopy measurements and then verified with HRTEM, with the patterns shown in Fig. 5. In XRD measurement of both MWCNT and CB, two characteristic peaks are detected at around 26° and 44° corresponding to {002} and {100} planes of graphitic carbon. The crystallite parameters L_c and d_{002} value for CNT and CB are 10.38 & 8.65 nm and 0.342 & 0.354 nm, respectively. Higher intensity peak and closer d-spacing value to ideal graphitic crystal layer interspacing (0.335 nm) imply the higher degree of graphitization of carbon material. The degree of graphitization of CNT being higher essentially means that CNT are composed of coaxial cylinders. The higher d-spacing and lower L_c-value indicate an evidently poorly crystallized graphitic structure of CB. The structural characterization of CNT using Raman spectroscopy was done by analyzing the resulting characteristic G-band and D-bands. The G-band (∼ at 1580 cm^{-1}) in graphitic materials arises due to in-plane tangential stretching of carbon-carbon bonds in ordered sp^2-bonded carbon, while D-band (∼ at 1340 cm^{-1}) is attribute to the presence of defects, disorder carbon and edges.[50,51] The ratio of intensity of D-band to G-band (I_D/I_G) is taken as degree of disorder in graphitic materials.[51] The I_D/I_G ratio for carbon black was 0.938 which was higher than that of CNT (0.780). Therefore, the degree of graphitization of CNT was higher than that of CB. Thus, the Raman spectrum data underpin the XRD results. Fig. 4c depict the high-resolution TEM (HRTEM) image of the pristine MWCNT with an average number of walls of about 30. Clearly, the as received CNT are free from metal contaminations and there are a limited number of defects on the tube sidewalls. Fig. 4d shows typical HRTEM image of carbon black. The carbon black displays a solid spherical particle of onion-peel like morphology that is composed of turbostratic graphitic structure. The magnified image of the lattice fringes are also shown that can readily resolve the intergraphene spacing of ca. 0.348 nm for the {002} plane which is consistent with the XRD and Raman results.

To demonstrate the effect of conductive additives (CNT and CB individually and CNT-CB as a hybrid filler) on electrical conductivity of MCMB electrode, the values of conductivity are plotted versus nano-filler contents as shown in Fig. 5. The total filler content in the composite electrodes was kept at 4 wt% as earlier studies have suggested no significant improvement in conductivity on increasing mass

Downloaded on 2017-09-28 to IP 103.27.9.249 address. Redistribution subject to ECS terms of use (see ecsdl.org/site/terms_use) unless CC License in place (see abstract).

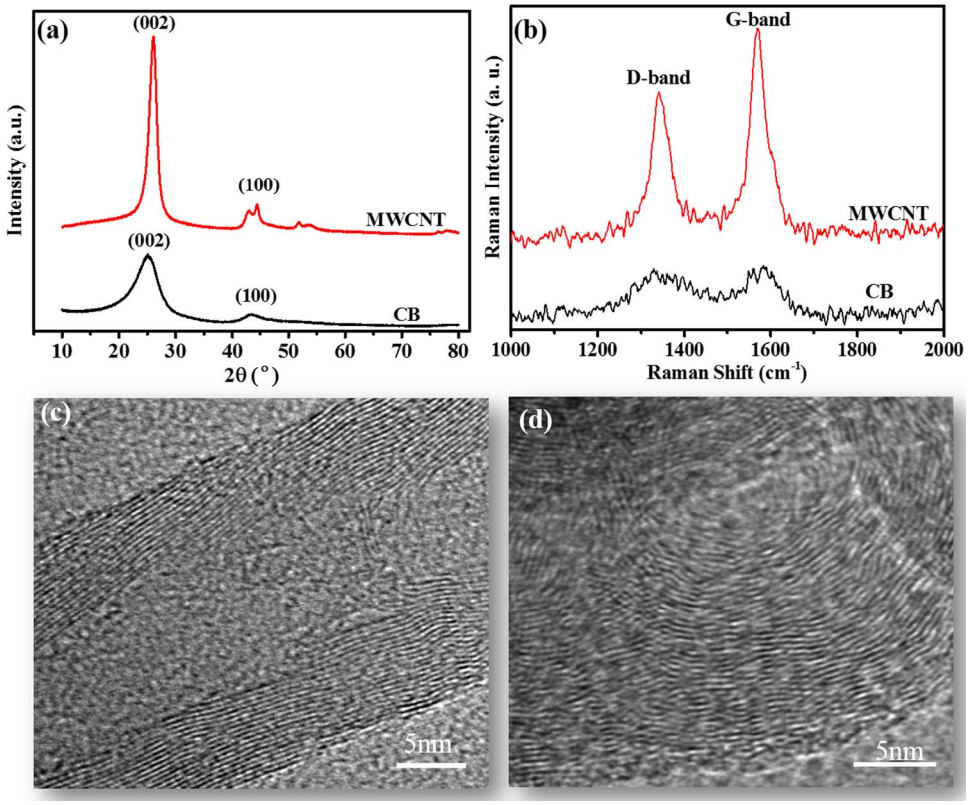

Figure 4. (a) XRD patterns of MWCNT and CB, (b) Raman spectra of MWCNT and CB, (c) HRTEM image of MWCNT and (d) HRTEM image of CB.

content of conductive additives.[31,52] An increase in electrical conductivity can be observed with gradual replacement of CB with CNT. This figure shows that the value of electrical conductivity of MCMB electrode without any additives is 2.13 ± 0.3 S-cm^{-1}. On addition of 4 wt% CB conducting fillers, the value of conductivity increases to 3.39 ± 0.2 S-cm^{-1} because the nano-size CB filler occupy the micron size voids available between MCMB particles leading to enhancement in conductivity of electrode composite. When 1 wt% of CB content is replaced by CNT, a steep increase in electrical conductivity to 5.04 ± 0.3 S-cm^{-1} occurs. Such a significant improvement is a result of higher conductivity of CNT, formation of hybrid conducting network that meets both the long-range and short-range conduction requirement. Moreover, the gap between CNT-CNT, MCMB-CNT and MCMB-MCMB are effectively filled as the various phases are linked together resulting in an efficient conducting network in which CB acts as an agent binding all phases together. Further replacement of CB with CNT leads to marginal change in the conductivity. This shows that the nanocomposite electrode has already attained the percolation limit and substituting more CB with CNT shows a negative effect on conductivity of composite electrode. Moreover, on completely substituting CB with CNT, a decline in conductivity value to 4.36 ± 0.6 S-cm^{-1} is observed. This reduction is caused by the agglomeration of CNT, fewer contacts between active material and CNT due to very high aspect ratio of CNT and improper contacts between CNT-CNT and MCMB-CNT.

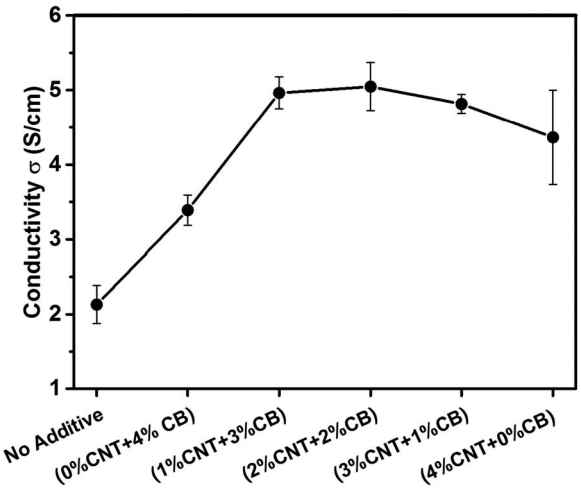

Figure 5. Electrical conductivity of composite electrode at various composition of conducting additive.

Furthermore, the conducting hybrid network of CNT-CB in MCMB composite electrodes is examined by the SEM images shown in Fig. 6 that illustrates the dispersion of nano-fillers in electrode matrix. For the electrode containing CNT only (Fig. 6a), it was observed that a conducting network is formed due to a random dispersion. However, at some places CNT tended to agglomerate with one another and therefore an efficient conducting network with full utilization of CNT material is not achieved. In case of electrodes with CB (Fig. 6b), the distribution of particles is in the form of congregate of nanoparticles to form a localized conducting network rather than a long-range string-like conducting pathway. Moreover, due to point-to-point connection, CB particulate cannot form a mechanically robust interconnected conductive network. As shown in Fig. 6c, by incorporating a hybrid filler through linking of CNT and CB into the MCMB electrode, the dispersion of nano-fillers were in such a manner that the CB particles occupy the gap between MCMB-MCMB MCMB-CNT and CNT-CNT forming short-range electrical pathways while the CNT form long-range pathways by connecting to multiple particles of active material. Hence, the CB spherules in conductive network constructed by hybrid fillers (CNT and CB) effectively join the active material and CNT as well as different CNT forming a solid three-dimensional conducting scaffold that provides an efficient electron pathway.

Downloaded on 2017-09-28 to IP 103.27.9.249 address. Redistribution subject to ECS terms of use (see ecsdl.org/site/terms_use) unless CC License in place (see abstract).

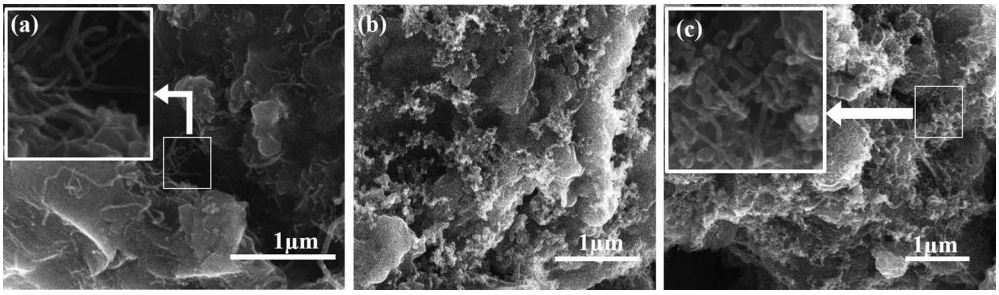

Figure 6. Distribution of conducting additives in MCMB electrodes (a) CNT agglomerate occur in only CNT as additive (b) CB filler a better dispersion (c) CNT-CB hybrid, CNT are connected through CB agglomerate in composite electrode.

Electrochemical characterization.—The influence of conductive additives on the electrochemical performances in carbon electrode were examined with 2016-type coin cells in which lithium foil was used as counter and reference electrode. Fig. 7 shows the typical cyclic voltammogram (CV) of MCMB electrode for various proportions of conductive fillers. The cyclic voltammetry was performed over a voltage range of 0.0–2.0 V vs. Li/Li^+ at a scan rate of 0.1 mVs^{-1}. Due to slight variation in weight between different electrodes prepared in this work, the current has been normalized with respect to the mass of active material for the sake of meaningful comparison in the CV curve. The MCMB electrode exhibits few peaks during anodic and cathodic polarization between 0.0–2.0 V. The redox peaks in voltammogram are characteristics of the electrode that correspond to the Li^+ insertion and extraction. It is shown in Fig. 7 that the anodic peak for electrode with CB filler was at 0.268 V and the corresponding cathodic peaks were at 0.167 V and 0.055 V. When CB was replaced with the same amount of CNT, the cathodic peak potential values remain nearly unaltered while the anodic peak value changes to 0.246 V. This reduction in anodic potential with CNT indicate a better conduction network because of higher conductivity and large aspect ratio of CNT that leads to lesser polarization of carbon electrode during lithiation/delithiation. This gap between anodic and cathodic peaks reduces further by using hybrid CNT-CB nano-fillers, in which the anodic peak potential changes to 0.220 V whereas a small but significant change in cathodic peak potential values leads to 0.178 V and 0.066V as shown in Fig. 7. This can again be attributed to the formation of highly efficient conductive network on using extremely different aspect ratio conducting fillers that leads to a better contact between active material and conductive additives. Such a network provides good conduction, smaller polarization and excellent intecalation/deintercalation reversibility.

Although not shown here, it was observed that MCMB electrode exhibits a discharge capacity of ca. 190 $mAhg^{-1}$ without any conducting agent implying the necessity of adding fillers. The charging/discharging current profile for the electrochemical characterization of half-cells is shown in Fig. 8. According to this, the cells were cycled between cutoff voltages with a constant current charge (C/4, 1C or 4C), followed by constant voltage charge until the charging current decayed to C/20, and finally constant current discharge at the same rate.[49] The plots for cycling performance of MCMB carbon electrodes with CB, CNT and CB-CNT hybrid conducting fillers at 0.25C, 1C and 4C-rate (*x*C-rate implies that one mole of Li react with one mole of C_6 in *1/x* hours) are shown in Fig. 9. It can be seen from Fig. 9a that the electrode containing 4 wt% CB as additive display an initial discharge capacity of 337.4 $mAhg^{-1}$ at 0.25C-rate. After 50 cycles the carbon electrode exhibits capacity retention of 96%. On replacing the CB-filler with the same amount of CNT, the electrode shows an improved initial capacity of 342.2 $mAhg^{-1}$ (Fig. 9a) and capacity retention of 97.0% after 50 cycles. This improvement in initial capacity and capacity retention for CNT nano-filler composite electrode is attributed to the outstanding intrinsic electronic conductivity of CNT and the formation of a robust conducting network with interlaced nanotubes. On the other hand, partially replacing CB with CNT forming a CB-CNT hybrid filler in various proportions of CB and CNT e.g., 3:1, 2:2 and 1:3 in electrodes, resulted in a dramatic improvement in initial discharge capacity as well as capacity retention capability. For instance, the electrode with hybrid CB-CNT fillers in 1:3 ratio demonstrated an initial discharge capacity of 352.8 $mAhg^{-1}$ with capacity retention ca. 98% after 50 cycles. The other compositions of CB-CNT hybrid fillers such as 2:2 and 3:1 exhibit initial capacity of 349.3 $mAhg^{-1}$ and 347.4 $mAhg^{-1}$, respectively with almost 98% capacity retention after 50 cycles as is shown in Fig. 9a.

In addition to the cycling performance at slow rate, the high-rate cycling performance of MCMB electrodes with CB, CNT and various proportions of CB-CNT hybrid additives was also studied. It was found that electrodes of mixed hybrid conducting fillers perform enormously better at 1C-rate and 4C-rate as is shown in Figs. 9b and 9c, respectively. For example, the initial capacity and capacity retention for MCMB-4%CB electrode at 1C-rate and 4C-rate after 100 cycles are demonstrated to be 330.4 $mAhg^{-1}$ and 84.6% and 305.3 $mAhg^{-1}$ and 73.1%, respectively. Whereas for MCMB-4%CNT, the initial capacity and capacity retention at 1C-rate are 335.9 $mAhg^{-1}$ and 86.9% and at 4C-rate are 309.2 $mAhg^{-1}$ and 82.1%, respectively after 100 cycles. On the other hand, the initial capacity and capacity retention for the electrodes with hybrid CB-CNT fillers in proportion

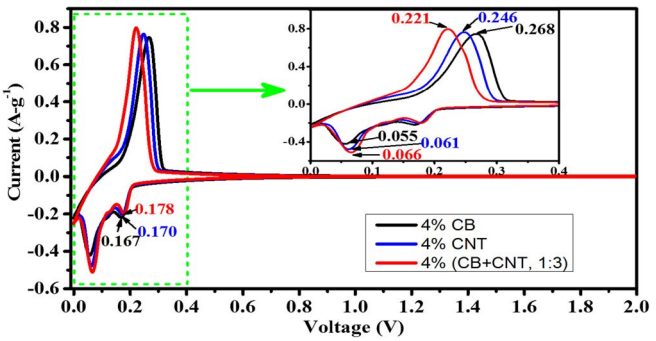

Figure 7. Cyclic voltammetry curves of MCMB electrodes for various conducting additives CB, CNT and hybrid CB-CNT at a scan rate of 0.1 mVs^{-1}.

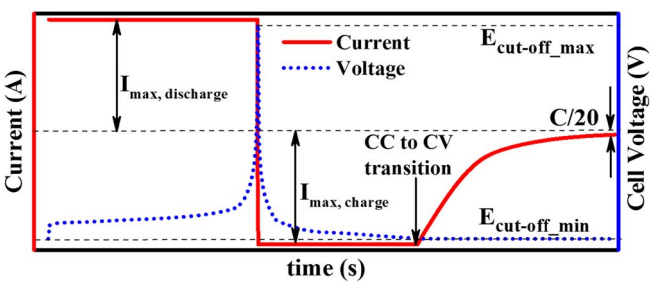

Figure 8. Representative current and cell voltage profile for galvanostatic cycling of Lithium-ion cells.

Downloaded on 2017-09-28 to IP 103.27.9.249 address. Redistribution subject to ECS terms of use (see ecsdl.org/site/terms_use) unless CC License in place (see abstract).

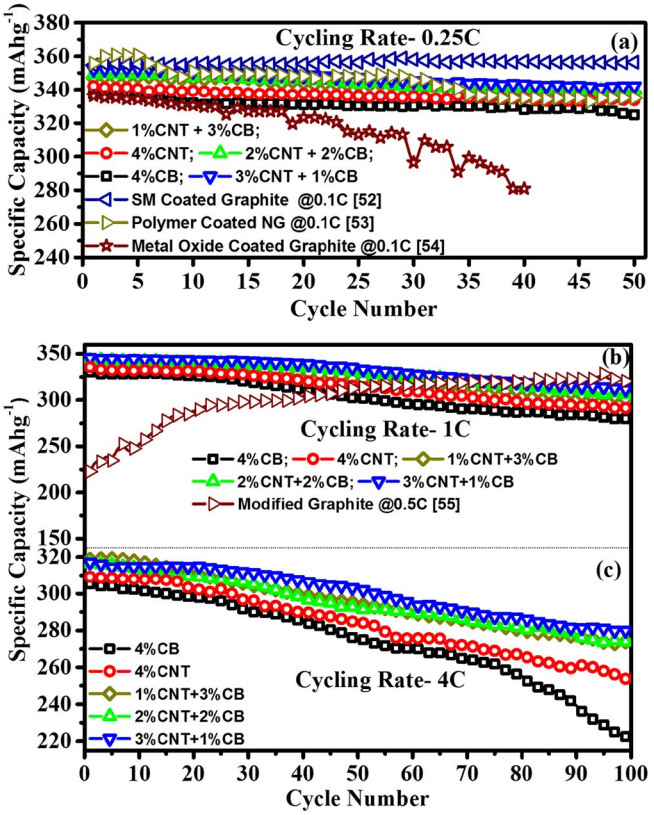

Figure 9. Cycling performances of MCMB electrodes with carbon black (CB), MWCNT and carbon black (CB) + MWCNT conducting additives at (a) 0.25C-rate, (b) 1C-rate and (c) 4C-rate and a comparison with state-of-the-art electrodes.[52–55]

of 1:3, 2:2, 3:1 are shown to be 346.2 $mAhg^{-1}$, 341.7 $mAhg^{-1}$, 341.0 $mAhg^{-1}$ and 90.1%, 89.7% and 88.3%, respectively at 1C-rate and 317.7 $mAhg^{-1}$, 316.8 $mAhg^{-1}$, 319.2 $mAhg^{-1}$ and 88.2%, 86.6% and 86%, respectively at 4C-rate. Recently, other carbonaceous electrode materials have been shown to exhibit much lower initial discharge capacity at high rate cycling. For example, the initial discharge capacity with N-doped porous carbon cycled at 2C and 5C rates has been reported to be 146 and 102.7$mAhg^{-1}$,[41] whereas with hollow carbon nanoparticle it was 266.3 $mAhg^{-1}$ at 1600 mAg^{-1} (4.3C-rate).[39]

Some graphitic anodes with high initial capacities have also been used to benchmark results obtained in this work. Shi et al.[52] studied the effect of sodium maleate (SM) coating on graphite particles in stablizing the SEI layer, maximize coulombic efficiency and extend cycle life. Li et al.[53] studied graphitic material based on a multi-functional polymer-blend coating to form an artificial SEI (A-SEI) layer to improve battery safety, reversible capacity and cycle life. The performance of graphitic electrode coated with metal oxides (Al_2O_3, TiO_2) using atomic layer deposition (ALD)[54] and measurements from graphite modified with $LiAlO_2$[55] have also been reported.

In Fig. 9, the capacity of MCMB electrode with nano-fillers is compared with these anode materials.[52–55] Specifically, we compare cycling performance of MCMB anode when cycled at 0.25C in Fig. 9a, and 1C in Fig. 9b. It can be observed that the initial capacity of SM coated graphite and polymer-blend graphite is quite similar with MCMB used in this work even though earlier measurements were done at 0.1C rate. The graphite electrode coated with metal oxides[54] shows lower initial capacity and significant fading over 50 cycles. Significantly, only the anode of Ref. 52 shows superior capacity retention than the electrodes fabricated in this work. Finally, the modified graphite electrode cycling performance (cycled at 0.5C rate)[55] when compared with MCMB electrodes with nano-fillers shows much lower initial capacity though the former's performance improves over 100 cycles where it becomes comparable to results obtained in the present work.

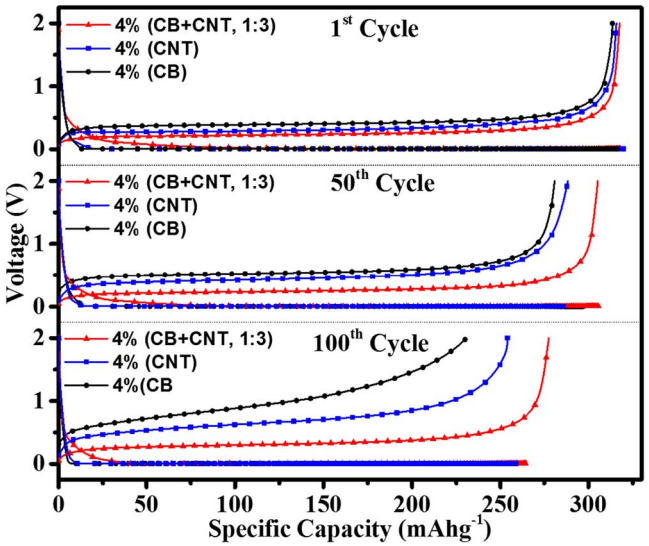

Figure 10. Charging-discharging performance of MCMB electrode for 1st, 50th and 100th cycle at 4C-rate with varying conducting agent.

Moreover, the coulombic efficiency in case of graphite anode with SM coating at 0.1C-rate was reported to be 90.9% at 0.1C,[52] whereas in our work with 1:3 (CB-CNT) additive carbon electrode it is 95% at 0.25C rate. Clearly, the initial discharge capacity and capacity retention (after 100 cycles) demonstrated by use of MCMB electrode with hybrid conducting additives in the ratio of 1:3 of CB-CNT in this work suggests improved performance and better utilization. This improvement in cycling performance and higher initial capacity for the electrodes containing combination of CB-CNT (with reference to electrode with CB only) is hence due to highly efficient electron-transfer at different scales and interfaces during charging/discharging even at high C-rate. This is the result of high aspect ratio CNT that form most of the conductive network and the small range gaps are effectively occupied by the CB spherules.

Furthermore, the charge-discharge profiles of 1st, 50th and 100th cycles of electrodes with CB, CNT and best performing hybrid CB-CNT (1:3) conducting filler are shown in Fig. 10. It can be seen that the electrode with hybrid conducting additives displays an extended voltage plateau after 100 cycles whereas in case of MCMB-CNT electrode a relatively low polarization is observed. In case of only CB as nano-filler electrode, the potential plateau suffers a huge deviation from the theoretical potential and the polarization becomes worse after 100 cycles as is shown in Fig. 10. The polarization value, which can be calculated in terms of potential difference between charge-discharge potential plateaus at the 100th cycle for the electrodes containing CB, CNT and CB-CNT fillers were 450 mV, 230 mV and 105 mV respectively. The high value of polarization of electrode with CB filler suggests that the interruption in conducting network which is merely based on point-to-point contact. During intercalation/deintercalation, a small expansion/contraction of MCMB particles take place that leads to the emergence of gaps among the adjacent MCMB particles with loss in contacts with different phases and hence failure of the conducting network. In contrast, for the electrodes containing CNT and hybrid CB-CNT conducting scaffold, negligible deviation and progressively low polarization signify a homogenous electrical contact due to uniform dispersion of CNT and formation of well-connected MCMB-CB-CNT chains that exhibit improved electrochemical kinetics for electrodes containing CNT and CB-CNT conducting fillers.

Electrochemical impedance spectroscopy.—Characterizing the effect of additives on kinetics of electrochemical processes involved, we have recorded the EIS spectra of electrodes with various nano-

Downloaded on 2017-09-28 to IP 103.27.9.249 address. Redistribution subject to ECS terms of use (see ecsdl.org/site/terms_use) unless CC License in place (see abstract).

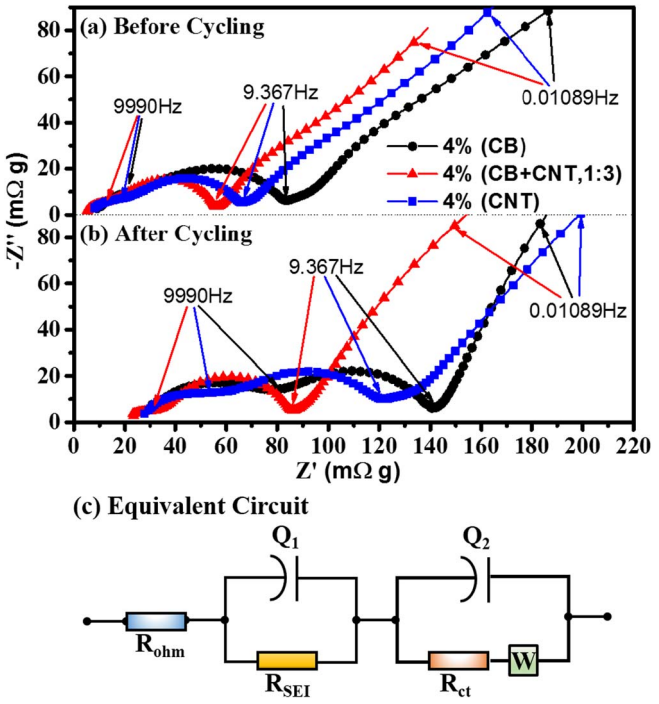

Figure 11. Impedance spectrum of MCMB electrode with different conducting additives at equilibrium potential of 0.2 V vs Li/Li$^+$ (a) before cycling (b) after 100 cycles at 1C-rate and (c) equivalent circuit used to fit the experimental EIS spectra.

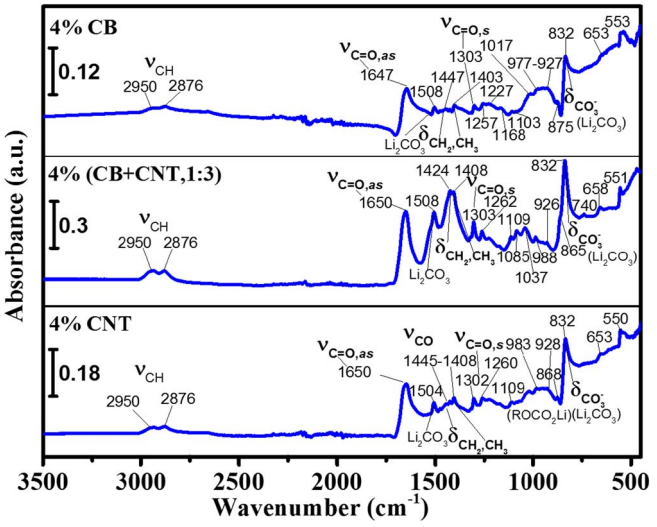

Figure 12. FTIR spectra of MCMB electrode with different conducting additives measured after the cells were charged/discharged for 100 cycles at 1C-rate.

fillers. It is known that EIS spectra and their semicircles are markedly defined at low voltage.[56] Therefore, all the impedance curves are recorded at 0.2 V OCP vs. Li/Li$^+$ for each electrode before and after cycling at 1C-rate. As shown in Figs. 11a and 11b, all the impedance spectra consist of two depressed semicircles in high to medium frequency range and a sloping line in a low frequency range. The depression in semicircles arise due to non-ideal capacitance behavior because of electrode surface roughness and porous microstructures.[57,58] The high frequency (10^6–10^4 Hz) depressed semicircle is assigned to lithium transfer through the solid electrolyte interface (SEI) film formed on the surface of MCMB carbon. The medium frequency (10^4–10^2 Hz) semicircle is generally ascribed to the charge transfer reaction and lithium transfer toward the carbon surface. At lower frequency, a sloping line is commonly attributed to the solid state diffusion of lithium into the graphitic layers of carbon anode. For the sake of meaningful comparison of many electrodes with different kind of conducting additives, the impedance values are mass normalized.[59] For quantitative analysis of impedance growth due to cycling with different nano-fillers, we fitted the AC spectra to modified Randles equivalent circuit as shown in Fig. 11c. R_{ohm} is associated to ohmic resistance which comprises the resistance due to electrolyte, electrodes, current collector and electrode interface and separator. R_{SEI} and Q_1 are related to resistance and constant phase element (CPE) of surface film formed on the carbon electrode, respectively. R_{ct} and Q_2 signify the charge-transfer resistance and CPE of double layer, respectively. W is Warburg impedance element attributed to solid state diffusion of Li$^+$. The fitting values of resistance for respective elements in the cell model for different nano-filler electrodes are shown in Figs. 11a and 11b and summarized in Table I. It can be seen that the resistance due to surface film after cycling is smaller for hybrid filler electrode than the other electrodes with CNT or CB as a filler. Also, the charge transfer resistance for mixed fillers electrode reduces significantly. This is attributed to the formation of dense, thin and more ionically conductive surface film for mixed fillers electrode that can pave the way for rapid diffusion of Li$^+$, good electron transfer and better kinetics in the electrode. Moreover the lesser ohmic resistance in case of hybrid fillers electrode suggests good conducting pathway. Also, from Table I, R_{ct} value for hybrid conducting additives electrode (47.35 mΩ-g) is much smaller than electrode with CB as additive (62.16 mΩ-g). This improvement in R_{ct} is attributed to the more easy electron and ion transfer between active material surface and electrolyte.

Ex-situ characterization.—The above ideas on the nature of SEI layer and its influence on cyclability of electrodes having various kind of nano-fillers have been verified by doing the post-mortem analysis using Fourier transform infrared (FTIR) spectroscopy. The SEI layer is formed on the surface of active material due to the reduction of electrolyte solution, with the reduction reaction ceasing only when the film is thick enough to prevent electron tunnelling. An ideal surface layer can be characterized as electronically insulated, high lithium permeability, small thickness (of few Å), dense, and resilient toward volumetric stresses.[60–62] Therefore, the layer formed plays a critical role in deciding rate capability, life and capacity retention.[60] Before IR-measurements, the half-cells for MCMB-CB, MCMB-CNT and MCMB-(CB-CNT) electrodes were charged/discharged for 100 cycles at 1C-rate in EC:DMC (1:1)/$LiPF_6$ 1M solution after stabilizing at slow rate (C/4). The IR-spectra, including the assignment of key peaks of molecular vibration in the range of 3500 cm^{-1}–450 cm^{-1} based on previous studies,[60,63,67–69] are shown in Fig. 12. The surface

Table I. Results of various resistances associated with surface film, species transfer and ohmic losses.

	R_{ohm} (mΩ-g)		R_{SEI} (mΩ-g)		R_{ct} (mΩ-g)		W (Ω-g-s$^{1/2}$)	
Conducting fillers	Before cycling	After cycling	Before cycling	After cycling	Before cycling	After cycling	Before cycling	After cycling
CB	9.07	30.69	22.56	48.0	60.44	62.16	13.45	17.36
CNT	7.85	27.63	18.84	39.6	46.81	60.81	12.2	14.83
CB-CNT	5.12	22.73	10.04	25.32	40.31	47.35	10.8	17.54

Downloaded on 2017-09-28 to IP 103.27.9.249 address. Redistribution subject to ECS terms of use (see ecsdl.org/site/terms_use) unless CC License in place (see abstract).

film formation can be ascribed using the absorbance spectra in which the major components are alkyl carbonates, the traces of lithium carbonates and lithium alkoxy moieties formed with the reduction of the carbonate solvent (EC).[60,64,65] As demonstrated from Fig. 11, species such as $(CH_2OCO_2Li)_2$ (peaks at 1650, 1450–1400, 1303, 1100–1070 and 832 cm^{-1}), ROLi (peaks at 2950–2876, 1080–1000 and 600–550 cm^{-1}) and Li_2CO_3 (peaks at 1510–1480 and 875–865 cm^{-1}) are formed on the surface of carbon electrode with different conductive additives. The spectra for all three composition exhibit peaks attributed to $(CH_2OCO_2Li)_2$, ROLi and Li_2CO_3 but differ in their relative intensity. The most intense absorbance peaks in IR-spectra are observed for electrode with CNT and CB hybrid conducting additive. This signifies a dense and stable SEI film formation on the surface of active material of electrode with hybrid nano-fillers. This is further ascribed to homogeneous electronic contacts derived from well-dispersed CNT and bridging the gaps between various CNT and MCMB-CNT particles with CB (Fig. 5c) forming a more robust and strain susceptible conducting network.[30] In the case of MCMB-CB electrode, a weak IR-spectra is observed that can be attributed to the porous and mechanically unstable SEI layer formation. This is because the CB spherules alone are unable to provide a continuous electronic network due to their heterogeneous distribution among MCMB particles as shown in Fig. 5b. In such a case, the electrode potential varies spatially owing to the variation in ohmic drop due to inhomogeneous conductivity. This leads to the nonuniform electrochemical reaction rate on the electrode surface resulting in formation of porous and unstable SEI film.[66] In contrast, when CNT is used as the additive, its scaffold not only hosts the active material but also buffers the change in volume of active material particles that occurs during charging/discharging process. The entire structure of conducting network remains intact even after many cycles signifying a relatively stable conducting scaffold that results in a reasonably dense and quite stable surface layer on MCMB carbon. Therefore, the IR-spectra for CNT mixed electrode is intense than electrode with CB-fillers but less in intensity from electrode having CB-CNT hybrid fillers.

Role of network structure.—A schematic description concerning the role of conducting fillers in improving the electrical and electrochemical performance of MCMB electrode is shown in Fig. 13. CB particles (Fig. 13a), due to their smaller size (20–30 nm) and spherical geometry build a conducting network on point-to-point contact basis that provide short-range electron pathways. However, high surface energy CB spherules tends to form an agglomerate locally rather than form a string like conducting network to develop a continuous conducting scaffold. These physical connections between CB-MCMB and CB-CB particles break during intercalation/deintercalation as a result of change in volume of active material. In the past, Reynier et al.[72] using in situ X-ray measurement observed that interparticle volume of electrode crystallite changes during intercalation/deinercalation of Li^+. This expansion has been reported to be up to 10% for lithiated graphite.[70–72] We measured a change of about 12–15% in thickness of the electrode after cycling for 50 cycles at 4C rate which corroborates the volume expansion of active material due to repeated intercalation/deintercalation and formation of an SEI layer. Further, a comparison of SEM images of fresh and cycled anode, shown in Fig. 14, demonstrates the formation of a surface layer with cracks due to cycling. The appearance of these cracks also indicates toward the loss of electrical contact between MCMB particles. Consequently,

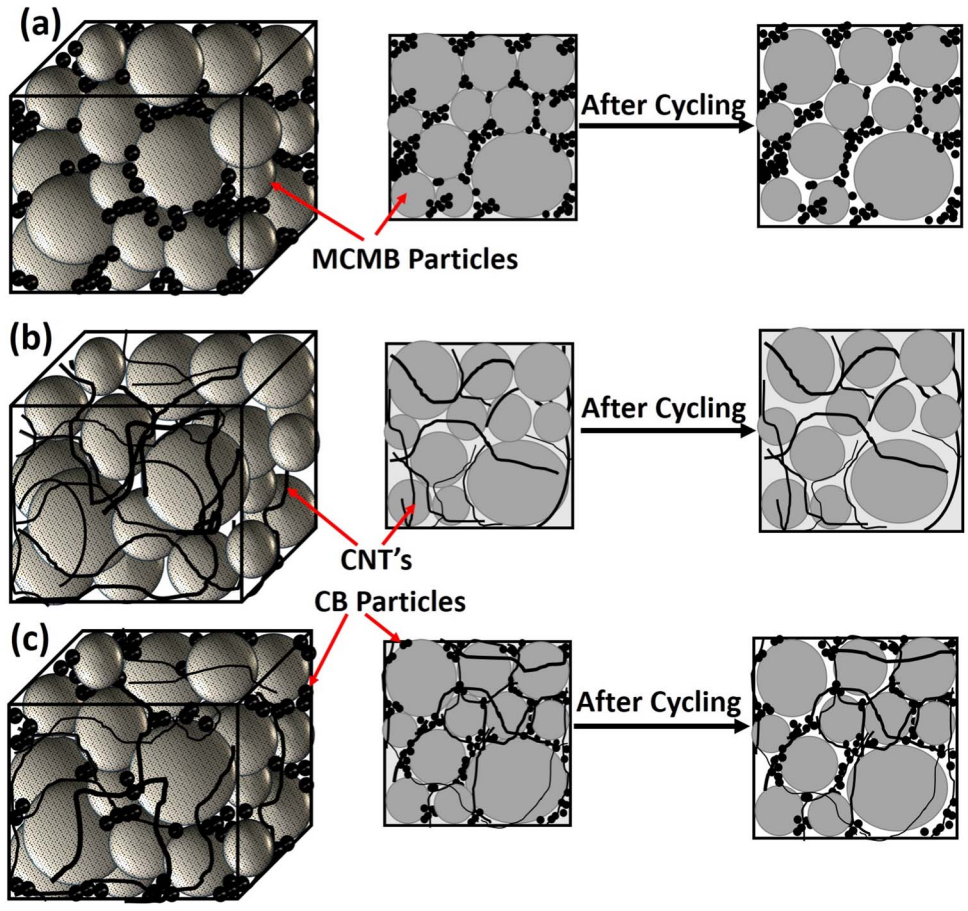

Figure 13. Schematic illustration of conducting network in 3D and 2D format (a) carbon black (CB) (b) carbon nanotubes (CNT) and (c) hybrid CB-CNT network for MCMB carbon electrode. The presence of gaps shown in post-cycling behavior schematics is visually exaggerated to explain the expansion and contraction due to repeated intercalation/deintercalation in MCMB.

Downloaded on 2017-09-28 to IP 103.27.9.249 address. Redistribution subject to ECS terms of use (see ecsdl.org/site/terms_use) unless CC License in place (see abstract).

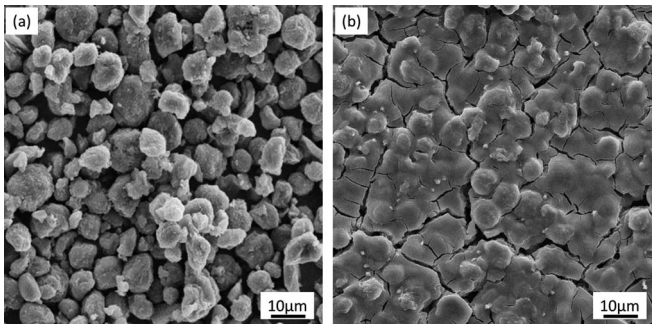

Figure 14. SEM images of (a) fresh electrode, and (b) an electrode cycled at 4C rate for 50 cycles. Cracks on the surface of cycled electrode is an evidence for the repeated change in volume of active material during intercalation/deintercalation.

the SEM images along with measurement of the electrode thickness provides support to our hypothesis that even though loss of electrical contact and cyclable lithium occurs due to cycling, the presence of CB-CNT compensates by providing pathways for fast electron conduction in these hybrid electrodes.

Moreover, the electrodes in which MCMB spheres are mixed with nanosize CB spherules render a low porosity, as the voids among various micron size particles are filled with these spherules thereby hampering the infiltration of liquid electrolyte and leading to large polarization particularly at high rate applications. In contrast, the scaffold formed by well dispersed CNT displays a highly conducting long-range electron pathway and highly porous medium through which liquid electrolyte percolate easily and leads to a reduction in electrical polarization as shown in Fig. 13b. However, CNTs alone offer a limited number of contacts and lower electronic conductivity along *c-axis.* However, it is inadmissible to discard the CB altogether as a combination of CB and CNT offer short- and long-range hybrid network with optimum porosity as is illustrated in Fig. 13c. In the hybrid network, CNT provide the primary conductive pathways (Fig. 13b) and CB act as a binding agent to tightly connect MCMB-CNT, CNT-CNT and MCMB-MCMB to build a π-conjugated environment throughout the composite electrode. Consequently, the developed hybrid scaffold synergistically promote the electron transfer at different scales. Such a strategy has also been successfully applied to polymer nanocomposite system to enhance the thermal and electrical conductivity, piezoresistive sensitivity, supercapacitor, lithium-ion battery cathodes, lithium-sulfur and lithium-air batteries.[5,27,31]

Conclusions

A promising strategy to develop carbon anode with improved rate capability by using an approach to hybridize the geometrically distinct shape, aspect ratio and different dispersion characteristic conducting nano-fillers (CB & CNT) was presented. A three-dimensional conducting scaffold formed by mixing 1% and 3% by weight of CB and CNT, respectively, provides better short-range and long-range conducting pathways, sufficient contact with MCMB active particles and a three-dimensional network. Therefore, experimental results for composite electrode display a synergistic improvement in electrical conductivity, initial capacity, capacity retention and stability. The MCMB electrode with such hybrid conducting fillers exhibit a higher electronic conductivity (≈5 S/cm). The electrochemical performance by use of different aspect ratio additives yields an initial capacity 352.8 $mAhg^{-1}$ and capacity retention value ca. 98% after 50 cycles at 0.25C-rate. At high currents, the hybrid CB-CNT conducting network performance is remarkably good, showing 280 $mAhg^{-1}$ initial capacity and 88.3% capacity retention at 4C-rate after 100 cycles. The performance of hybrid electrodes was compared with those containing CB or CNT fillers only and post-mortem analysis using FTIR, a surface sensitive technique, was conducted to study the constituents of the SEI formed with different compositions of additives. The results with CB-CNT hybrid additives in 1:3 weight ratio signify not just faster electronic conduction in the electrode but also a thin and mechanically stable SEI, well-connected network and good adhesion of various phases of composite electrode are the factors leading to the significant improvement in electrochemical performance of MCMB electrode. This kind of strategy, i.e., tailoring the conducting network by using geometrically different conducting fillers can also be applied to polymer nanocomposite system to enhance the thermal and electrical conductivity, piezoresistive sensitivity, in supercapacitors, Lithium-ion battery cathodes, Lithium-sulfur and Lithium-air batteries.

Acknowledgment

Financial support from Council of Scientific & Industrial Research (CSIR) under 22/648/13/EMR-II is gratefully acknowledged.

References

1. J. Bisquert, G. Garcia-Belmonte, P. Bueno, E. Longo, and L. O. S. Bulhoes, "Impedance of constant phase element (CPE)-blocked diffusion in film electrodes," *J. Electroanal. Chem.*, **452**, 229 (1998).
2. A. Varzi, C. Täubert, M. Wohlfahrt-Mehrens, M. Kreis, and W. Schütz, "Study of multi-walled carbon nanotubes for lithium-ion battery electrodes," *J. Power Sources*, **196**, 3303 (2011).
3. H. Y. Tran, G. Greco, C. Täubert, M. Wohlfahrt-Mehrens, W. Haselrieder, and A. Kwade, "Influence of electrode preparation on the electrochemical performance of $LiNi_{0.8}Co_{0.15}Al_{0.05}O_2$ composite electrodes for lithium-ion batteries," *J. Power Sources*, **210**, 276 (2012).
4. A. Ghosh, S. Shukla, G. S. Khosla, B. Lochab, and S. Mitra, "Sustainable sulfur-rich copolymer/graphene composite as lithium-sulfur battery cathode with excellent electrochemical performance," *Sci. Rep.*, **6**, 25207 (2016).
5. K. Wang, Y. Wu, S. Luo, X. He, J. Wang, K. Jiang, and S. Fan, "Hybrid super-aligned carbon nanotube/carbon black conductive networks: A strategy to improve both electrical conductivity and capacity for lithium ion batteries," *J. Power Sources*, **233**, 209 (2013).
6. S. E. Cheon, C. W. Kwon, D. B. Kim, S. J. Hong, H. T. Kim, and S. W. Kim, "Effect of binary conductive agents in $LiCoO_2$ cathode on performances of lithium ion polymer battery," *Electrochim. Acta*, **46**, 599 (2000).
7. M. Koltypin, V. Pol, A. Gedanken, and D. Aurbach, "The Study of carbon-coated V_2O_5 nanoparticles as a potential cathodic material for Li rechargeable batteries," *J. Electrochem. Soc.*, **154**, A605 (2007).
8. M. Yoshio, H. Wang, K. Fukuda, Y. Hara, and Y. Adachic, "Effect of Carbon Coating on Electrochemical Performance of Treated Natural Graphite as Lithium-Ion Battery Anode Material," *J. Electrochem. Soc.*, **147**, 1245 (2000).
9. H. Momose, H. Honbo, S. Takeuchi, K. Nishimura, T. Horiba, Y. Muranaka, Y. Kozono, and H. Miyadera, "X-ray photoelectron spectroscopy analyses of lithium intercalation and alloying reactions on graphite electrodes," *J. Power Sources*, **68**, 208 (1997).
10. K. Nishimura, H. Honbo, S. Takeuchi, T. Horiba, M. Oda, M. Koseki, Y. Muranaka, Y. Kozono, and H. Miyadera, "Design and performance of l0Wh rechargeable lithium batteries," *J. Power Sources*, **68**, 436 (1997).
11. Y. P. Wu, E. Rahm, and R. Holze, "Effects of heteroatoms on electrochemical performance of electrode materials for lithium ion batteries," *Electrochim. Acta*, **47**, 3491 (2002).
12. R. Tossici, M. Berrettoni, M. Rosolen, and R. Marass, "Electrochemistry of KC_8 in lithium-containing electrolytes and its use in lithium-ion cells," *J. Electrochem. Soc.*, **144**, 186 (1997).
13. C. Fu, C. Song, L. Liu, X. Xie, and W. Zhao, "Synthesis and properties of nitrogen-doped graphene as anode materials for lithium-ion batteries," *Int. J. Electrochem. Sci.*, **11**, 3876 (2016).
14. W. J. Lee, U. N. Maiti, J. U. M. Lee, J. Lim, T. H. Han, and S. O. Kim, "Nitrogen-doped carbon nanotubes and graphene composite structures for energy and catalytic applications," *Chem. Commun.*, **50**, 6818 (2014).
15. N. Liu, Z. Lu, J. Zhao, M. T. McDowell, H.-W. Lee, W. Zhao, and Y. Cu, "A pomegranate-inspired nanoscale design for large-volume-change lithium battery anodes," *Nat. Nano*, **9**, 187 (2014).
16. F. Joho, B. Rykart, R. Imhof, P. Novak, M. E. Spahr, and A. Monnier, "Key factors for the cycling stability of graphite intercalation electrodes for lithium-ion batteries," *J. Power Sources*, **81**, 243 (1999).
17. S. Yang, H. Song, and X. Chen, "Electrochemical performance of expanded mesocarbon microbeads as anode material for lithium-ion batteries," *Electrochem. Commun.*, **8**, 137 (2006).
18. E. Peled, C. Menachem, D. Bar-Tow, and A. Melman, "Improved graphite anode for lithium-ion batteries," *J. Electrochem. Soc.*, **143**, L4 (1996).
19. T. Takamura, M. Saito, A. Shimokawa, C. Nakahara, K. Sekine, S. Maeno, and N. Kibayashi, "Charge/discharge efficiency improvement by the incorporation of conductive carbons in the carbon anode of Lithium-ion batteries," *J. Power Sources*, **90**, 45 (2000).

Downloaded on 2017-09-28 to IP 103.27.9.249 address. Redistribution subject to ECS terms of use (see ecsdl.org/site/terms_use) unless CC License in place (see abstract).

20. X. L. Li, K. Du, J. M. Huang, F. Y. Kang, and W. C. Shen, "Effect of carbon nanotubes on the anode performance of natural graphite for lithium ion batteries," *J. Phys. Chem. Solids*, **71**, 457 (2010).
21. J. H. Lee, G. S. Kim, Y. M. Choi, W. I. Park, J. A. Rogers, and U. Paika, "Comparison of multiwalled carbon nanotubes and carbon black as percolative paths in aqueous-based natural graphite negative electrodes with high-rate capability for lithium-ion batteries," *J. Power Sources*, **184**, 308 (2008).
22. X. Li, F. Kang, and W. Shen, "Multiwalled carbon nanotubes as a conducting additive in a $LiNi_{0.7}Co_{0.3}O_2$ cathode for rechargeable lithium batteries," *Carbon*, **44**, 1334 (2006).
23. J. Zhang, Z. Xie, W. Li, S. Dong, and M. Qu, "High-capacity grapheneoxide/graphite/carbon nanotube composites for use in Lithium-ion battery anodes," *Carbon*, **74**, 153 (2014).
24. D. J. Yang, S. G. Wang, and Q. Zhang, "Thermal and electrical transport in multi-walled carbon nanotubes," *Phys. Rev. Lett.*, **329**, 207 (2004).
25. C. A. Frysz, X. Shui, and D. D. L. Chung, "Carbon filaments and carbon black as a conductive additive to the manganese dioxide cathode of a lithium electrolytic cell," *J. Power Sources*, **58**, 41 (1996).
26. W. Guoping, Z. Qingtang, Y. Zuolong, and Q. M. Zheng, "The effect of different kinds of nano-carbon conductive additives in lithium ion batteries on the resistance and electrochemical behavior of the $LiCoO_2$ composite cathodes," *Solid State Ionics*, **179**, 263 (2008).
27. Y. Liu, X. Li, H. Guo, Z. Wang, W. Peng, Y. Yang, and R. Liang, "Effect of carbon nanotube on the electrochemical performance of C-$LiFePO_4$/graphite battery," *J. Power Sources*, **184**, 522 (2008).
28. J. H. Du, J. Bai, and H. M. Cheng, "The present status and key problems of carbon nanotube based polymer composites," *Express Polym. Lett.*, **1**, 253 (2007).
29. M. Buttiker, "Four-terminal phase-coherent conductance," *Phys. Rev. Lett.*, **57**, 1761 (1986).
30. I. V. Thorat, V. Mathur, J. N. Harb, and D. R. Wheeler, "Performance of carbon-fiber-containing $LiFePO_4$ cathodes for high-power applications," *J. Power Sources*, **162**, 673 (2006).
31. K. Ke, P. Pötschke, N. Wiegand, B. Krause, and B. Voit, "Tuning the network structure in poly (vinylidene fluoride)/carbon nanotube nanocomposites using carbon black: Toward improvements of conductivity and piezorestive sensitivity," *ACS Appl. Mater. Interfaces*, **8**, 14190 (2016).
32. S. M. Zhang, L. Lin, H. Deng, X. Gao, E. Bilotti, T. Peijs, Q. Zhang, and Q. Fu, "Synergistic effect in conductive networks constructed with carbon nanofillers in different dimensions," *Express Polym Lett*, **6**, 159 (2012).
33. J. Sumfleth, X. C. Adroher, and K. Schulte, "Synergistic effects in network formation and electrical properties of hybrid epoxy nanocomposites containing multiwall carbon nanotubes and carbon black," *J. Mater. Sci.*, **44**, 3241 (2009).
34. P. C. Ma, M. Y. Liu, H. Zhang, S. Q. Wang, R. Wang, K. Wang, Y. K. Wong, B. Z. Tang, S. H. Hong, K. W. Paik, and J. K. Kim, "Enhanced electrical conductivity of nanocomposites containing hybrid fillers of carbon nanotubes and carbon black," *ACS Appl. Mater. Interfaces*, **1**, 1090 (2009).
35. Z. S. Wu, W. Ren, L. Xu, F. Li, and H. M. Cheng, "Doped graphene sheets as anode materials with superhigh rate and large capacity for lithium ion batteries," *ACS Nano*, **5**, 5463 (2011).
36. B. J. Landi, M. J. Ganter, C. D. Cress, R. A. DiLeo, and R. P. Raffaelle, "Carbon nanotubes for lithium ion batteries," *Energy Environ. Sci.*, **2**, 638 (2009).
37. C. Li, X. Yin, L. Chen, Q. Li, and T. Wang, "Porous carbon nanofibers derived from conducting polymer: Synthesis and application in lithium-ion batteries with high-rate capability," *J. Phys. Chem. C*, **113**, 13438 (2009).
38. H. Wang, T. Abe, S. Maruyama, Y. Iriyama, Z. Ogumi, and K. Yoshikawa, "Graphitized carbon nanobeads with an onion texture as a lithium-ion battery negative electrode for high-rate use," *Adv. Mater.*, **17**, 2857 (2005).
39. C. Ma, J. Dong, Y. Zhao, J. Li, and H. Chen, "Dual-template synthesis of novel pomegranate-like hollow carbon nanoparticles with improved electrochemical performance for Li-ion batteries," *Carbon*, **110**, 180 (2016).
40. B. M. Way and J. R. Dahn, "The Effect of boron substitution in carbon on the intercalation of lithium in $Li_x(B_zC_{1-z})_6$," *J. Electrochem. Soc.*, **141**, 907 (1994).
41. X. Zhang, G. Zhu, M. Wang, J. Li, T. Lu, and L. Pan, "Covalent-organic-frameworks derived N-doped porous carbon materials as anode for superior long-life cycling lithium and sodium ion batteries," *Carbon*, **116**, 686 (2017).
42. Y. Wu, S. Fang, and Y. Jiang, "Carbon anode materials based on melamine resin," *J. Mater. Chem.*, **8**, 2223 (1998).
43. S. Flandrois and B. Simon, "Carbon material for lithium-ion rechargeable batteries," *Carbon*, **37**, 165 (1999).
44. Y. P. Wu, E. Rahm, and R. Holze, "Carbon anode material for lithium ion batteries," *J. Power Sources*, **114**, 228 (2003).
45. M. Endo, C. Kim, K. Nishimura, T. Fojino, and K. Miyashita, "Recent development of carbon material for Li ion batteries," *Carbon*, **38**, 183 (2000).
46. K. Presson, V. A. Sethuraman, L. J. Hardwick, Y. Hinuma, Y. S. Meng, A. van der Ven, V. Srinivasan, R. Kostecki, and G. Ceder, "Lithium diffusion in graphitic carbon," *J. Phys. Chem. Lett.*, **1**, 1176 (2010).
47. Y. Yamada, K. Miyazaki, and T. Abe, "Role of edge orientation in kinetics of electrochemical intercalation of Lithium-ion of graphite," *Langmuir*, **26**, 14990 (2010).
48. K. Dokko, N. Nakata, Y. Suzuki, and K. Kanamura, "High-rate lithium deintercalation from lithiated graphite single-particle electrode," *J. Phys. Chem. C*, **114**, 8646 (2010).
49. M. Rashid and A. Gupta, "Experimental assessment and model development of cycling behavior in Li-ion coin cells," *Electrochim. Acta*, **231**, 171 (2017).
50. A. C. Ferrari and J. Robertson, "Interpretation of Raman spectra of disordered and amorphous carbon," *Phys. Rev. B*, **61**, 14095 (2000).
51. F. Tuinstra and J. L. Koenig, "Raman spectrum of graphite," *J. Chem. Phys.*, **53**, 1126 (1970).
52. Q. Shi, W. Liu, Q. Qu, T. Gao, Y. Wang, G. Liu, V. S. Battaglia, and H. Zheng, "Robust solid/electrolyte interphase on graphite anode to suppress lithium inventory loss in lithium-ion batteries," *Carbon*, **111**, 291 (2017).
53. F.-S. Li, Y.-S. Wu, J. Chou, M. Winter, and N.-L. Wu, "A mechanically robust and highly ion-conductive polymer-blend coating for high-power and long-life lithium-ion battery anodes," *Adv. Mater.*, **27**, 130 (2015).
54. H.-Y. Wang and F.-M. Wang, "Electrochemical investigation of an artificial solid electrolyte interface for improving the cycle-ability of lithium ion batteries using an atomic layer deposition on a graphite electrode," *J. Power Sources*, **233**, 1 (2013).
55. Y. Wu, Y.-F. Li, L.-Y. Wang, Y.-J. Bai, Z.-Y. Zhao, L.-W. Yin, and H. Li, "Enhancing the Li-ion storage performance of graphite anode material modified by $LiAlO_2$," *Electrochim. Acta*, **235**, 463 (2017).
56. Y. Cai and C.-L. Fan, "Influences of conductive additives on electrochemical performances of artificial graphite anode with different shapes for lithium ion batteries," *Electrochim. Acta*, **58**, 481 (2011).
57. D. Aurbach, B. Markovsky, I. Weissman, E. Levi, and Y. Ein-Eli, "On the correlation between surface chemistry and performance of graphite negative electrodes for Li ion batteries," *Electrochim. Acta*, **45**, 67 (1999).
58. E. Peled, D. Golodnitsky, and G. Ardel, "Advanced model for solid electrolyte interphase electrodes in liquid and polymer electrolytes," *J. Electrochem. Soc.*, **144**, L208 (1997).
59. R. Alcantara, G. F. Ortiz, P. Lavela, and J. L. Tirado, "EPR, NMR, and electrochemical studies of surface modified carbon microbeads," *Chem. Mater.*, **18**, 2293 (2006).
60. S. J. An, J. Li, C. Daniel, D. Mohanty, S. Nagpure, and D. L. Wood, "The state of understanding of the lithium-ion-battery graphite solid electrolyte interphase (SEI) and its relationship to formation cycling," *Carbon* ,**105**, 52 (2016).
61. A. Tokranov, B. W. Sheldon, P. Lu, X. Xiao, and A. Mukhopadhyay, "The origin of stress in the solid electrolyte interphase on carbon electrodes for Li ion batteries," *J. Electrochem. Soc.*, **161**, A55 (2014).
62. A. Mukhopadhyay, F. Guo, A. Tokranov, X. Xiao, R. H. Hurt, and B. W. Sheldon, "Engineering of grphene layer orientation to attain high rate capability and anisotropic properties in Li-ion battery electrode," *Adv. Funct. Mater.*, **23**, 2397 (2005).
63. K. Xu, "Nonaqueous liquid electrolytes for lithium-based rechargeable batteries," *Chem. Rev.*, **104**, 4303 (2004).
64. R. Marom, O. Haik, D. Aurbach, and I. C. Halalay, "Revisiting $LiClO_4$ as an electrolyte for rechargeble lithium-ion batteries," *J. Electrochem. Soc.*, **157**, A972 (2010).
65. P. Verma, P. Maire, and P. Novak, "Review of the features and analyses of the solid electrolyte interphase in lithium-ion batteries," *Electrochim. Acta*, **55**, 6332 (2010).
66. T. Takamura, M. Saito, A. Shimokawa, C. Nakahara, K. Sekine, S. Maeno, and N. Kibayashi, "Charge/discharge efficiency improvement by the incorporation of conductive carbons in the carbon anode of Lithium-ion batteries," *J. Power Sources*, **90**, 45 (2000).
67. J. P. Gabano, *Lithium batteries*, Academic Press, London, 1983.
68. P. B. Balbuena and Y. Wang, *Lithium-ion batteries: Solid-electrolyte interphase*, Imperial College Press, London, 2004.
69. Y. Ein-Eli, B. Markovsky, D. Aurbach, Y. Carmeli, H. Yamin, and S. Luski, "The dependence of the performance of Li-C intercalation anodes for Lithium-ion secondary batteries on the electrolyte solution composition," *Electrochim. Acta*, **39**, 2559. (1994)
70. D. Billaud, E. McRae, and A. Hérold, "Synthesis and electrical resistivity of lithium-pyrographite intercalation compounds (stages I, II and III)," *Mater. Res. Bull.*, **14**, 857 (1979).
71. Y. Qi, "Threefold increase in the Young's modulus of graphite negative electrode during lithium intercalation," *J. Electrochem. Soc.*, **157**, A558 (2010).
72. Y. Reynier, R. Yazami, and B. Fultz, "XRD evidence of macroscopic composition inhomogeneities in the graphite-lithium electrode," *J. Power Sources*, **165**, 616 (2007).

Downloaded on 2017-09-28 to IP **103.27.9.249** address. Redistribution subject to ECS terms of use (see **ecsdl.org/site/terms_use**) unless CC License in place (see abstract).